Journal of Catalysis 361 (2018) 222–229

Contents lists available at ScienceDirect

Journal of Catalysis

journal homepage: www.elsevier.com/locate/jcat

Functionalizing carbon nitride with heavy atom-free spin converters for enhanced $^1O_2$ generation

Wenting Wu [a,b], Congcong Han [a], Qinhua Zhang [a], Qinggang Zhang [a], Zhongtao Li [a], David J. Gosztola [b], Gary P. Wiederrecht [b,*], Mingbo Wu [a,*]

[a] State Key Laboratory of Heavy Oil Processing, College of Chemical Engineering, China University of Petroleum (East China), Qingdao 266580, People's Republic of China
[b] Center for Nanoscale Materials, Argonne National Laboratory, Argonne, IL 60439, USA

ARTICLE INFO

Article history:
Received 13 December 2017
Revised 2 March 2018
Accepted 5 March 2018
Available online 26 March 2018

Keywords:
Carbon nitride
Heavy atom-free spin converters
Singlet oxygen
Intersystem crossing
Selective photooxidation

ABSTRACT

Carbon nitride as a metal-free conjugated polymer exhibits an intriguing prospect for the design of advanced photosensitizers for singlet oxygen ($^1O_2$) generation. However, the intersystem crossing (ISC) process is quite insufficient in carbon nitride, limiting the $^1O_2$ generation. Here, we report a facile and general strategy to confined benzophenone as a heavy atom-free spin converter dopant in carbon nitride via the facile copolymerization. With proper energy level matching between the heavy atom-free spin converter and various ligands based on carbon nitride precursors, the proper combination can decrease the singlet-triplet energy gap (ΔE_{ST}) and hence generate $^1O_2$ effectively. Due to its significant and selectivity for $^1O_2$ generation, the as-prepared carbon nitride-based photosensitizer shows a high selective photooxidation activity for 1,5-dihydroxy-naphthalene (1,5-DHN). The product yield reached 71.8% after irradiation for 60 min, which was higher than that of cyclometalated Pt^{II} complexes (53.6%) in homogeneous photooxidation. This study can broaden the application of carbon nitride in the field of selective heterogeneous photooxidation due to simple operation, low cost, and high efficiency, making it a strong candidate for future industrialization.

1. Introduction

Singlet oxygen ($^1O_2$) has proven to be an effective oxygen species for many selective organic syntheses, such as selective oxidation of primary alcohols to aldehydes [1] and conversion of anthracene derivatives to anthraquinone [2]. As a result, there is a need to efficiently create $^1O_2$ for these and other reactions, beginning with the $^3O_2$ ground state. One route is through the use of $^1O_2$ photosensitizers that improve photon absorption and also demonstrate efficient intersystem crossing (ISC) [3]. As shown in Scheme 1, $^1O_2$ photosensitizers work by first undergoing photoexcitation into a singlet excited state. These photosensitizers then undergo the crucial ISC process, so that the triplet state can sensitize oxygen through triplet-triplet energy transfer (TTET) [3–5]. Therefore, an efficient ISC process is the crucial factor for enhancing $^1O_2$ generation. Previously, heavy atoms, such as Pt(II) [6,7], Ru(II) [8], I and Br [9,10], were used as spin converters to induce the ISC process. Unfortunately, it is limited by high cost, low quantum yield, easy photobleaching and nonrecyclability. Recently, metal-free conjugated polymers based on carbon nitride exhibited an intriguing prospect for photooxidation [11–13]. However, there remain few rational design strategies for these conjugated polymers to selectively enhance $^1O_2$ generation.

Incorporation of functional groups with carbon nitride that undergo efficient ISC, otherwise known as heavy atom-free spin converters, is a facile and inexpensive way to selectively enhance $^1O_2$ generation [14,15]. For example, benzophenone with a low-lying n-π^* transition is a good candidate for the spin converter due to large spin-orbit coupling, and its ISC efficiency can reach 100% [16,17]. However, chemical modification with ligands often induces an unpredictable change of photochemical properties, such as alteration of the singlet-triplet energy gap (ΔE_{ST}) [18,19]. It is known that a smaller ΔE_{ST} generally produces a more efficient ISC process and $^1O_2$ generation (Scheme 1) [20,21]. If the ligand unit, the moiety connected to the spin converter, has extremely large π conjugation, the low-lying transition would be π-π^* instead of n-π^*. This would increase ΔE_{ST} and prohibit the ISC process [22]. On the other hand, a ligand structure with less π conjugation could also influence ΔE_{ST}. Therefore, the proper ligand plays a very important role for the ISC process and $^1O_2$ generation.

* Corresponding authors.
E-mail addresses: wiederrecht@anl.gov (G.P. Wiederrecht), wumb@upc.edu.cn (M. Wu).

https://doi.org/10.1016/j.jcat.2018.03.006
0021-9517/

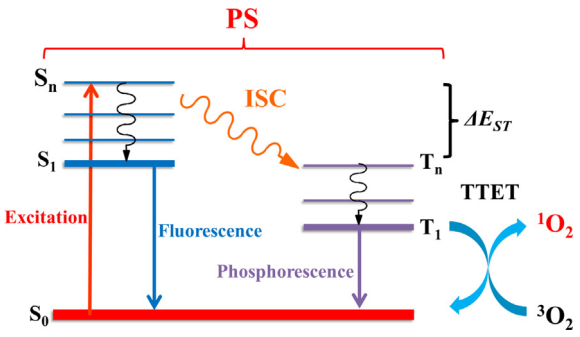

Scheme 1. The modified Jablonski diagram of the photoexcitation energy transfer process of a photosensitizer (PS) that undergoes efficient intersystem crossing (ISC) to enable triplet–triplet energy transfer (TTET) to generate singlet oxygen ($^1O_2$). The functionalization of PS with compounds that undergo ISC (spin converters) is one approach to producing $^1O_2$. The smaller singlet-triplet energy gap (ΔE_{ST}) benefits efficient ISC process and $^1O_2$ generation.

Based on this principle, we used precursors of carbon nitride (melamine and melem) as ligands of heavy atom-free spin converters (benzophenone) to explore their structure-property relationship for enhancing $^1O_2$ generation. The heavy atom-free spin converter doped carbon nitride was prepared via the facile copolymerization of 3,3′,4,4′-benzophenonetetracarboxylic dianhydride (it has the benzophenone structure to function as the spin converter) and a carbon nitride precursor. The structures were confirmed by TEM, SEM, solid-state ^{13}C NMR, XPS and XRD. The modified carbon nitride is shown to greatly enhance $^1O_2$ generation and selective photooxidation of 1,5-dihydroxynaphthalene (1,5-DHN). 1,5-DHN is a substance that contaminates water, but its product (5-hydroxy-1,4-naphthalenedione, Juglone) obtained after oxidation has hemostatic and antibacterial activity. Furthermore, ESR, steady state/time-resolved luminescence spectroscopy and DFT calculations were used to explore the structure-property relationship for enhancing $^1O_2$ generation. This work provides a basis for broadening the application of carbon nitride in the field of selective photooxidation due to simple operation, low cost and high efficiency. More importantly, the heterogeneous photocatalysis process enables the product to be easily obtained by simple filtration, which is beneficial for industrial applications.

2. Experimental

2.1. Materials preparation

3,3′,4,4′-benzophenonetetra-carboxylic dianhydride (BTDA), 3, 3,4,4′-biphenyltetracarboxylic dianhydride (BPDA) and melamine were obtained from Aladdin Industrial Corporation. All the chemicals in our experiment were directly used without further purification.

Melem was synthesized by heating melamine placed in a porcelain crucible with a cover at 425 °C for 4 h in a muffle furnace [23]. Similarly, graphitic carbon nitride (g-C_3N_4) was synthesized by heating melamine at 550 °C for 4 h in a muffle furnace [24].

Photocatalysts based on carbon nitride were synthesized by facile thermal condensation of melem and BTDA. In detail, 1 g of powder mixture of melem and BTDA (the molar ratios of melem and BTDA were 5:1, 3:1, 1:1, 1:3, 1:5, respectively) was put into a railboat and heated at 5 °C/min up to 300 °C for 4 h under the protection of N_2. The samples (the molar ratio of melem and BTDA at 1:1) were calcined under different temperature. The optimum temperature was chosen at 300 °C (Table S1). In order to avoid the influence of unreacted BTDA, the resultant block solid was treated with ultrasound and washed with N,N-dimethylformamide (DMF) three times. Finally, the light brown product denoted as CN-T was filtered and dried at 60 °C. Similarly, other control samples of CN-P (melem and BPDA without benzophenone structure were mixed at the ratio of 1:1) and ME-T (melamine and BTDA were mixed at the ratio of 1:1) were prepared using the same method.

2.2. Materials characterization

The morphologies of the samples were characterized by scanning electron microscopy (SEM) (Hitachi S-4800, Japan) and transmission electron microscopy (TEM) (JEM-2100UHR, Japan). XRD patterns were obtained on a powder X-ray diffractometer at 40 kV and 15 mA using Cu Kα radiation (X'Pert PRO MPD, Holland). X-ray photoelectron spectroscopy (XPS) measurements were performed on an ESCALAB 250Xi spectrometer equipped with a prereduction chamber. Solid-state ^{13}C nuclear magnetic resonance (^{13}C NMR) was measured on a Bruker Advance III 400 M spectrometer equipped with a 9.4 T magnet. The UV–Vis spectra were recorded on a UV–Vis spectrophotometer (UV-2700, Shimadzu, Japan). The $^1O_2$ emission signal of the CN-T photosensitizer was detected in a fluorescence spectrometer FLS980 (Edinburgh Instruments Ltd.) with a 450 W Xe lamp and a NIR detector. The sample was excited at 360 nm. The experimental conditions were excitation and emission bandwidths of 15 nm, integration time 2 s/step (0.1 s dwell time × 20 repeats) and step of 1 nm for the sample. The ns-domain time-resolved fluorescence spectra and the μs-domain time-resolved spectra were also obtained on an FLS980 fluorescence spectrometer (Edinburgh Instruments Ltd.). Triplet emission spectra and lifetimes were also characterized with a Horiba Jobin-Yvon fluorolog spectrometer system.

2.3. Photooxidation 1,5-DHN test

The photochemical reaction was performed at room temperature under air atmosphere in a round bottom flask (50 mL) with irradiation by a 35 W xenon lamp (600 W/m^2). The MeCN/H_2O (v/v = 5:1) mixed aqueous solution (20 mL) containing 1.0×10^{-4} mol/L of 1,5-DHN and photocatalysts (20.0 mg) was irradiated at λ > 385 nm (the light with a wavelength shorter than 385 nm was blocked by 0.72 M $NaNO_2$ solution). UV–Vis absorption spectra were used to record at intervals of 10 min. The consumption of 1,5-DHN was monitored by a decrease in the absorption at 331 nm, and the concentration of 1,5-DHN was calculated by using its molar extinction coefficient (ε = 7664 M^{-1} cm^{-1}). Juglone production at intervals of 10 min was monitored by an increase in the absorption peak at 419 nm. The concentration of Juglone was also calculated by using its molar extinction coefficient (ε = 3567 M^{-1} cm^{-1}), and the yield of Juglone was calculated according to the following eqn:

$$\text{Yield} = \frac{100 \times A_{i(\text{Juglone})}/\varepsilon_{(\text{Juglone})}}{C_{\text{initial}(1,5-\text{DHN})}} \times 100\%$$

$A_{i(\text{Juglone})}$ is the absorbance of Juglone in solution; $\varepsilon_{(\text{Juglone})}$ is the molar extinction coefficient of Juglone; $C_{\text{initial}(1,5\text{-DHN})}$ is the initial concentration of 1,5-DHN.

2.4. Electron spin resonance (ESR) spectroscopy

Electron spin resonance (ESR) spectra were recorded at room temperature using a JEOL JES FA200 spectrometer at 9.8 GHz, X-band, with 100 Hz field modulation. Samples were quantitatively injected into specially made quartz capillaries for ESR analysis in the dark and illuminated directly in the cavity of the ESR spectrometer. In the whole test process, 2,2,6,6-tetramethylpiperidine

(TEMP) and 5,5-dimethyl-1-pyrroline-N-oxide (DMPO) were selected as the trapping agents to examine $^1O_2$ and $O_2^{\cdot-}$ generation, respectively.

2.5. Theoretical calculations

All calculations were carried out with Gaussian 09. DFT calculations with B3LYP/6-31G basis set were used for ground state optimization of organic models. The energy levels of the S_n states (energy gap between S_0 and S_n) and T_n states (energy gap between S_0 and T_n) were calculated with time-dependent DFT (TDDFT) calculations on the basis of optimized ground state geometries.

3. Results and discussion

3.1. Morphology and structural characterization

CN-T was prepared by copolymerization of melem and BTDA with different molar ratios and the thermal condensation process as illustrated in Fig. 1a, wherein the anhydride group in BTDA prefers to react with the amino group in melem and produces the imide group in CN-T. This imide group could, to some extent, separate the melem and BTDA, and prevent the π conjugation. Based on the photooxidation performance, the optimized ratio is at 1:1 (vide infra). Thus, in this work CN-T was prepared at the ratio of 1:1 and other analogues were also prepared at this ratio in the following. Considering the contribution of benzophenone structure and the different energy levels of melem and melamine, in this work, other control samples of CN-P (melem and BPDA without benzophenone structure were mixed at the ratio of 1:1) and ME-T (melamine and BTDA were mixed at the ratio of 1:1) were prepared using the same method, as depicted in Fig. S1.

The morphology of CN-T and melem was investigated via scanning electron microscopy (SEM) and transmission electron microscopy (TEM). The SEM image of CN-T (Fig. 1c) displays a fragment-like structure after introducing BTDA, which is similar to the morphology of melem (Fig. 1b). The TEM images (Fig. S2) show that CN-T and melem are composed of some sheet-like structure, as is the case for the g-C_3N_4 [25,26].

The crystal and chemical structure of CN-T were first analyzed by X-ray diffraction (XRD), X-ray photoelectron spectroscopy (XPS) and solid-state ^{13}C NMR. Calcination at the experimental temperature did not affect the attribution of the peaks from the melem and BTDA in XRD and ^{13}C NMR (Fig. S3). Therefore, the original BTDA and melem before calcination can be used to characterize the structure. Melem shows a (1 0 0) peak at 2θ of 12.36, which can be attributed to the in-plane repeated tri-s-triazine units (Fig. S4) [27]. With the increasing ratio of BTDA in the CN-T samples, the peak at 2θ of 12.36 becomes weak and finally disappears as the ratio reaches 1:1. It indicates that BTDA completely reacts with melem and destroys the in-plane units. The strong shoulder peak at 2θ of 27.43 originates from the (0 0 2) interlayer diffraction of a graphitic-like structure [28]. Notably, when the amount of melem is greater, the peak at 2θ of 27.43 is overlapped, including the characteristic diffraction peak of BTDA. This proves that melem partly reacts with BTDA. Interestingly, a weakened (1 0 0) peak and a broadened (0 0 2) peak indicate the decreased crystallinity and weakened periodic structure of melem after BTDA was introduced.

^{13}C NMR spectrum of CN-T further confirmed its structure and the connection between BTDA and melem (Fig. 2) [29,30]. For BTDA, the signal at 194 ppm can be attributed to carbonyl groups (position 10). For CN-T, a weak signal at 194 ppm could also be observed without obvious shift. It indicates that the benzophenone structure was almost completely preserved, which benefits the ISC process and subsequent $^1O_2$ generation. For BTDA, the signal at 164 ppm (position 9), to some extent, has overlap with the peak of melem at position 2. So in the ^{13}C NMR spectrum of CN-T, it shows a broadband peak at around 164 ppm. Peaks at 154 ppm (position 1) and 125–142 ppm (position 3–8) are observed, which can be attributed to melem (position 1) and BTDA (position 3–8) respectively. Therefore, BTDA was successfully connected with melem in CN-T, meanwhile the benzophenone structure for the ISC process was finely reserved. These results were also confirmed by XPS (Fig. S5).

3.2. Detection of reactive oxygen species

In order to identify the generated reactive oxygen species (ROS) directly, photoluminescence and electron spin resonance (ESR) measurements were performed on both CN-T and melem. In the photoluminescence measurement, there is characteristic emission of $^1O_2$ at around 1265 nm from CN-T (Fig. 3a) indicating the $^1O_2$ generation [31,32]. 2,2,6,6-tetramethylpiperidine (TEMP) was selected as the trapping agent to examine $^1O_2$ generation in the system. As shown in Fig. 3b, the ESR signal for the CN-T clearly displays an intense 1:1:1 triplet signal with g-value of 1.9996 [32,33]. Compared with melem, the ESR signal from CN-T is much stronger than that of melem. Therefore, the incorporation of BTDA would greatly enhance the $^1O_2$ generation.

In addition, other ROS were also detected to exclude additional oxygen activation behaviors. Superoxide anion radicals ($O_2^{\cdot-}$) were detected via employing the 5,5-dimethyl-1-pyrroline-N-oxide (DMPO) as the trapping agent (Fig. S6a) [34]. It can be seen that a negligible amount of $O_2^{\cdot-}$ was detected for both CN-T and melem, and its influence on the selective oxidation is minimal. The detection of hydroxyl radicals (·OH) is typically accomplished by using coumarin as a probe molecule [35]. It can form 7-hydroxycoumarin with intense fluorescent emission as a result of reacting with ·OH. As shown in Fig. S6b, no significant increase of fluorescence was observed after 30 min of illumination, indicating

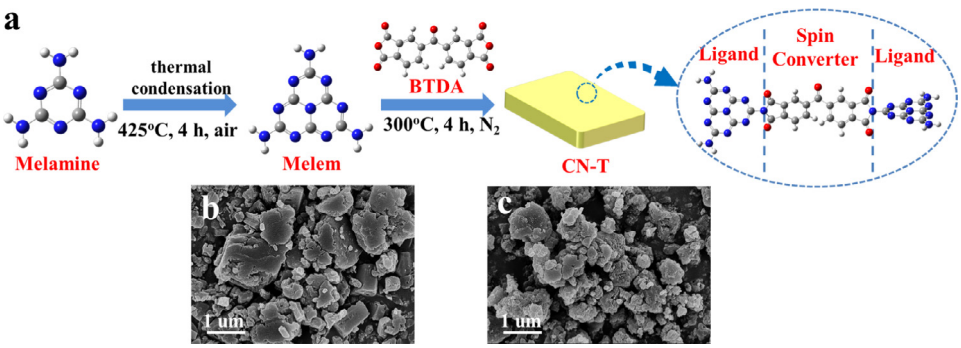

Fig. 1. (a) Synthesis procedure of porous CN-T and the SEM images of (b) melem and (c) CN-T.

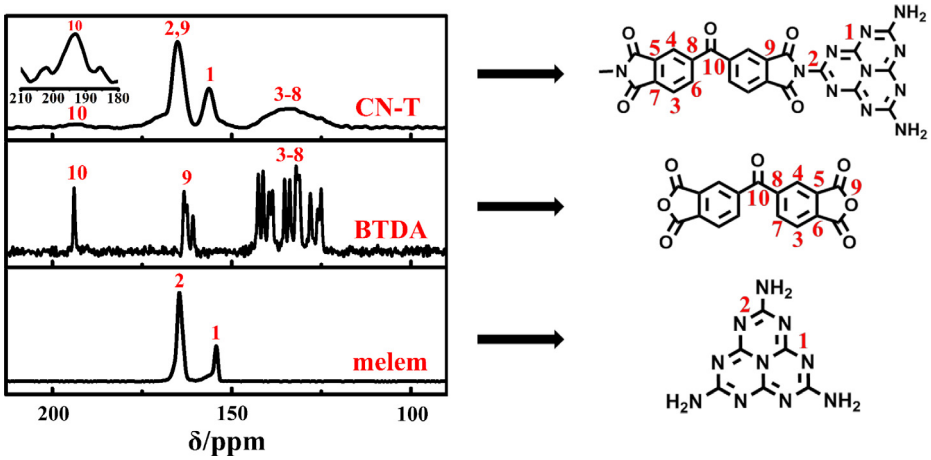

Fig. 2. ^{13}C NMR spectra and molecular structures of CN-T, BTDA and melem.

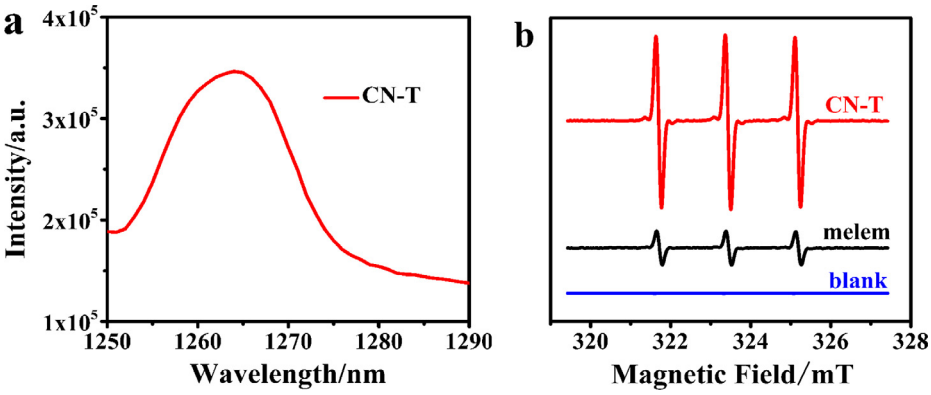

Fig. 3. (a) The $^1O_2$ emissions of CN-T under excitation with a Xe lamp; (b) ESR spectra of CN-T and melem upon irradiation for 12 min in the presence of TEMP.

that ·OH is not significantly generated in this system·H_2O_2 was detected by using KI/CH_3COOH/starch system [10]. A reddish brown color was observed when mixing the reaction system with KI/CH_3COOH/starch in the presence of H_2O_2. Fig. S7 shows that there is little H_2O_2 existence in the reaction system. Therefore, the $^1O_2$ generation was selectively enhanced, which would benefit for the selective photooxidation.

3.3. Photooxidation activities

UV–Vis diffuse reflectance spectra (DRS) of prepared samples (Fig. S8) shows that there is a clear red shift of the absorption in CN-T compared with BTDA (the absorption edge is at about 410 nm) and melem (the absorption edge is at about 450 nm), implying that the incorporation of BTDA could enhance the visible light harvesting ability and the subsequent the catalytic activity of CN-T. Furthermore, benefiting from its high selectivity and efficiency for $^1O_2$ generation, CN-T is expected to be an excellent photocatalyst for selective oxidation reactions. Herein, the photooxidation of 1,5-DHN was performed with CN-T as a photocatalyst, and the photooxidation process is shown in Fig. 4a. When the mixed solution of photosensitizer and 1,5-DHN is irradiated with a 35 W xenon lamp (600 W/m^2), the absorption of 1,5-DHN at 331 nm decreased and the absorption of the product Juglone at 425 nm increased (Fig. 4b, Fig. S9, Fig. S10). The product Juglone by self-sensitization can be negligible in experiment (Fig. S9a). For CN-T (the melem and BTDA at 1:1), the reaction rate of 1,5-DHN is the highest (Fig. S11) and the yield of Juglone could come to 71.8% after irradiation for 60 min, which is higher than other ratios (Fig. 4c). Compared with previous report about cyclometalated Pt^{II} complexes (53.6%) in homogeneous photooxidation [36], the yield of Juglone by the prepared heterogeneous photosensitizer was increased to a factor of 1.3 times. At the same time, its selectivity for Juglone is highest (Table S2). The photocatalytic stability of CN-T was also investigated in the following repeated experiments. As shown in Fig. 4d, when a concentrated solution of 1,5-DHN was added twice to the original solution, the yield of Juglone has no significant loss. However, there is a slight increase in the third cycle. This may be due to the accumulation of 1,5-DHN without completely reacting in the first two cycles. It indicates that CN-T has excellent photostability and photocatalytic ability. Besides, there was no physical or chemical change for CN-T photocatalyst after the photocatalytic reaction (Fig. S12).

After the photooxidation reaction, the crude product was dissolved in trichloromethane and the pure product could be obtained by simple filtration. The structure and purity of the product were detected by ^1H NMR. Other unreacted substances were mainly raw materials (1,5-DHN). As shown in Fig. S13, the ^1H NMR spectrum of prepared product shows the same characteristic peaks corresponding to those of commercial Juglone purchased from Aladdin Industrial Corporation, and no other peaks were observed. This result indicates that no other by-products were generated during this photooxidation. It also provides a simple method for the preparation of Juglone with high purity.

Further confirming the contribution of benzophenone structure, its analogue without ketone groups (3,3,4,4-biphenyltetracar

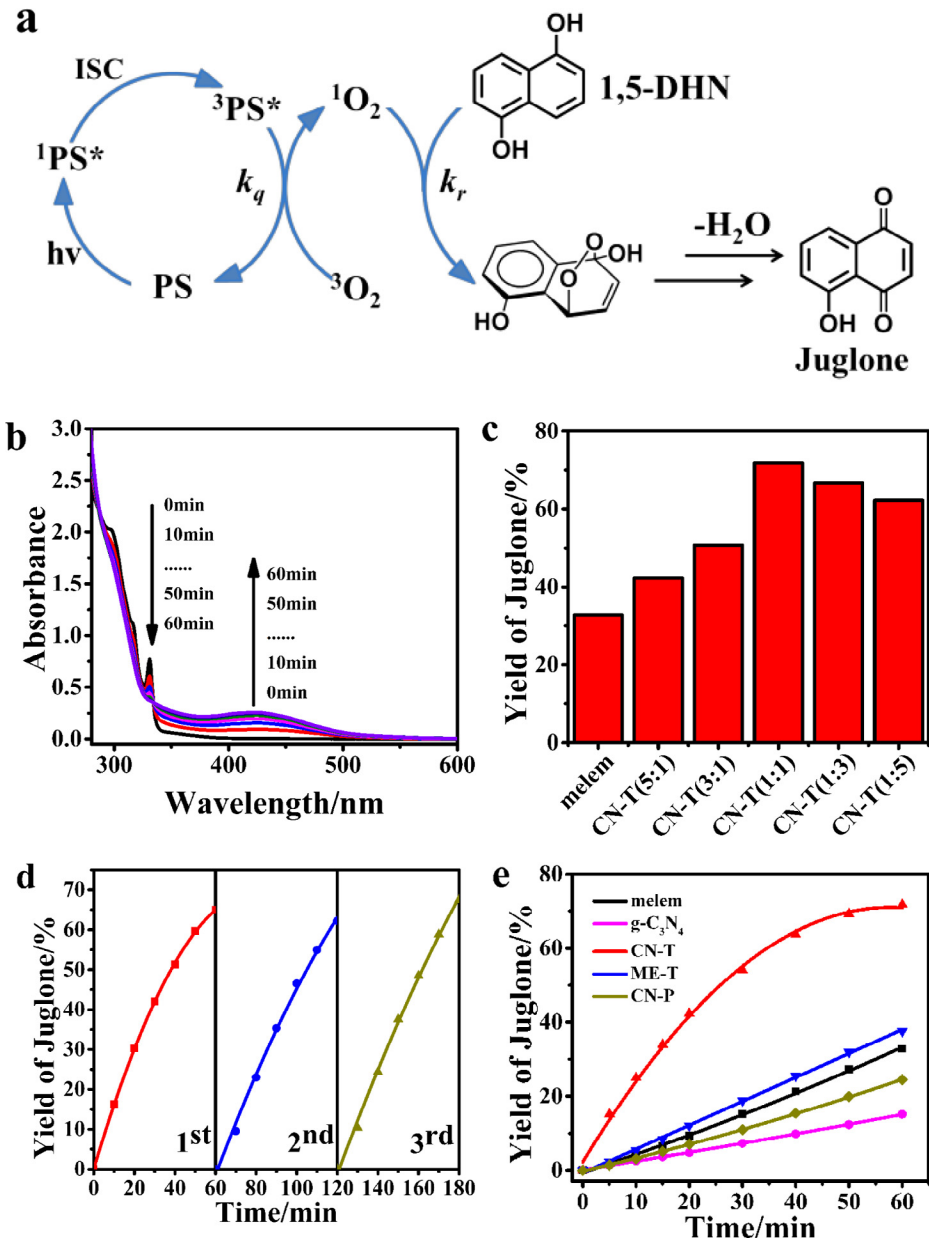

Fig. 4. (a) Mechanism for photooxidation of 1,5-DHN; (b) UV–vis absorption spectral change for the photooxidation of 1,5-DHN by CN-T; (c) The yield of Juglone by melem and different proportions of samples; (d) Stability of CN-T in photooxidation of 1,5-DHN; (e) The yield of Juglone by melem, CN-T and control samples.

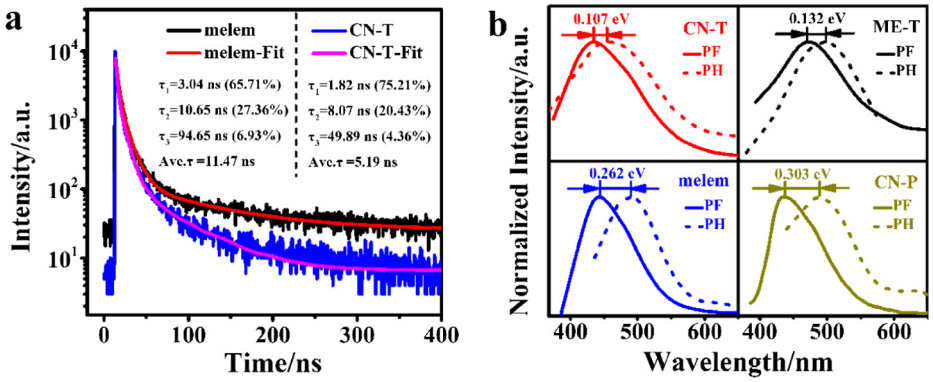

Fig. 5. (a) Time-resolved PF kinetics (excitation at 375 nm) of melem and CN-T. The solid lines show the fitting curves. The peak emissions for corresponding PF were monitored (Fig. S14a); (b) Normalized PF and PH spectras for CN-T, ME-T, CN-P and melem (excitation at 375 nm, 293 K). The faster decay of the PF in CN-T relative to melem is additional evidence that there is significant ISC in CN-T. The maximum emission peaks of PF and PH are listed in Table S3.

boxylic dianhydride, BPDA), was introduced to react with melem, and formed CN-P. But the yield catalyzed by CN-P was only 24.4% (Fig. 4e). For melem and g-C_3N_4, they don't have the benzophenone structure, and the relative catalysis product yields were only 32.8% and 15.1%, respectively (Fig. 4e). These results indicate that the benzophenone may function as a spin converter for ISC process and subsequent $^1O_2$ generation. Actually, the ligand connected to the spin converter is also important for further enhancing $^1O_2$ generation. For ME-T, it has a benzophenone structure in ME-T, and its yield was 37.6% (Fig. 4e). Although it is higher than those without the spin converter, its yield is about half of CN-T. The results demonstrate that both spin converter and ligand are responsible for the improvement of $^1O_2$ generation.

3.4. Photocatalytic mechanism investigation

In order to gain insight into the photocatalytic mechanism of the photosensitizer, we performed steady-state and time-resolved prompt fluorescence (PF) and phosphorescence (PH) measurements. As shown in Fig. 5a and Fig. S14b, the mean PF lifetime of CN-T was determined as 5.19 ns, which is shorter than CN-P without ketone structure (8.29 ns) and melem without benzophenone structure (11.47 ns). The obvious decrease of the mean PF lifetime may be related to the acceleration of the nonradiative ISC process in CN-T, suggesting a more effective conversion from the singlet into triplet excitons by the assistance of BTDA [11]. Herein, the occurrence of multiple lifetime components is most

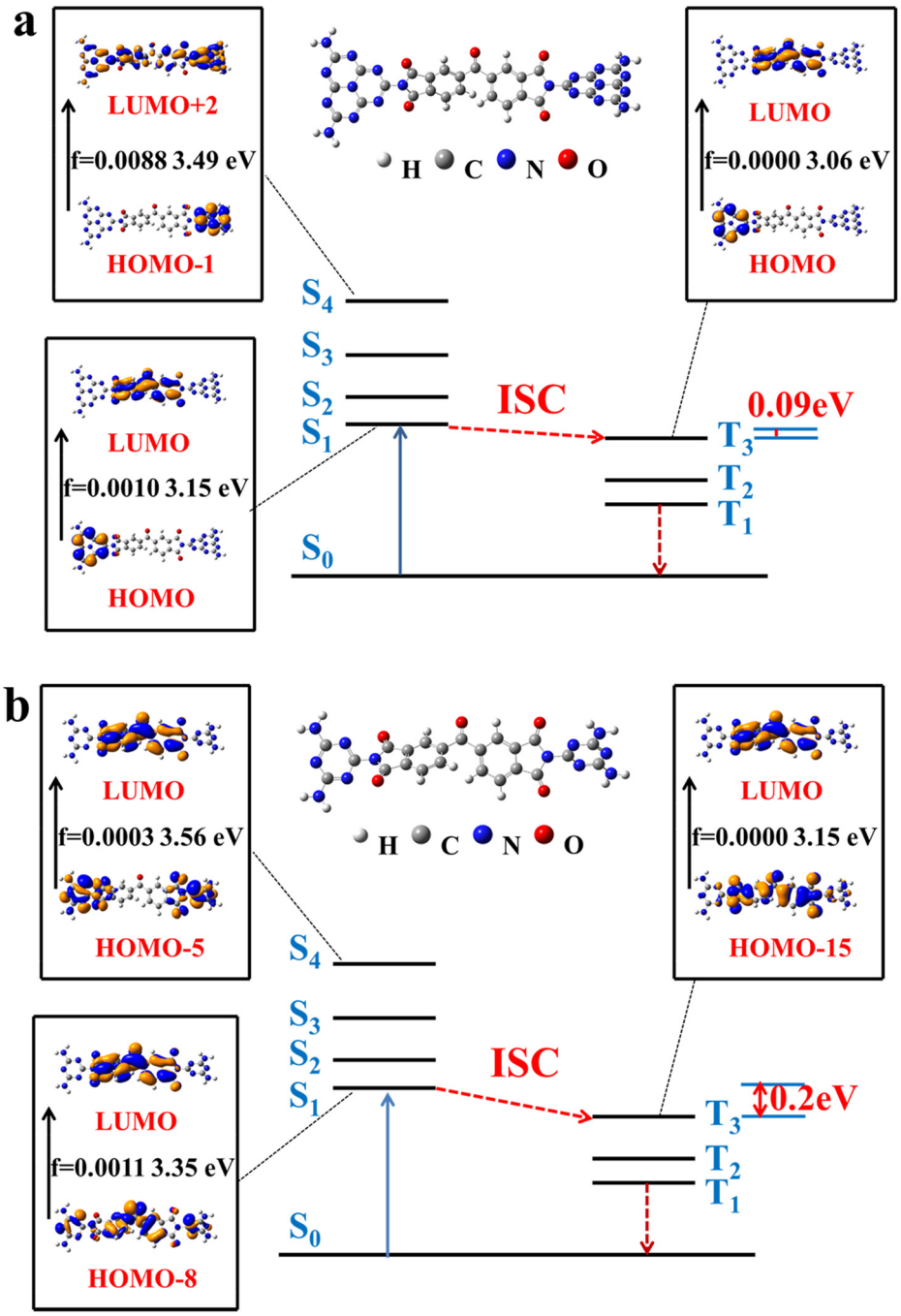

Fig. 6. Selected frontier molecular orbitals involved in the excitation and the singlet/triplet excited states of (a) CN-T and (b) ME-T. The left column is UV–Vis absorption (based on the ground state geometry) and the right column is the triplet excited state (based on the ground state geometry). For clarity, only the selected excited states were presented.

likely due to the heterogeneity of the polymer matrix or to fluorophore-fluorophore interactions[37]. For CN-T, the emission at 466 nm can be quenched by O_2 molecules. Compared with the emission under N_2 atomosphere, the phosphorescent emission was quenched 25.5% under air atmosphere (Fig. S14c). This quenching effect is less than traditional phosphorescence in solution, which may be due to the fact that sample powders have less surface contact to O_2 during the emission measurements. In addition, the emission lifetime of CN-T at 466 nm is 1.34 μs (Fig. S14d), which is longer than its fluorescence lifetime (5.19 ns). All of these results indicate that the emission at the longer wavelength can be attributed to the phosphorescence.

The ΔE_{ST} can be used to estimate the efficiency of the ISC process [11,17,38], which can be calculated by the PF and PH peak wavelengths. Given the distinct different lifetimes between PF and PH, the red-shifted PH spectra and PF spectra can be readily extracted from the time-resolved luminescent spectra. Based on the fluorescence lifetime, the emission disappears after a 1 μs delay time. Here, the luminescent spectra at 0 μs and 1 μs can be selected as the PF spectra and PH spectra respectively. As shown in Fig. 5b, CN-T has the smallest ΔE_{ST} values (0.107 eV), and the next one is ME-T (0.132 eV) following by melem (0.262 eV) and CN-P (0.303 eV). Therefore, the introduction of benzophenone structure could increase ISC efficiency, and the ligand will have further significant influence on it.

Meanwhile, taking into account the influence of ligands (melem and melamine), theoretical studies were performed by DFT/TDDFT calculations. The ground state geometries of the models were optimized using DFT methods with the B3LYP/6-31G basis set. The singlet state energy (S_n) and triplet state energy (T_n) were calculated with time dependent DFT (TDDFT) calculations [39]. DFT calculation results of CN-T and ME-T are in accordance with the absorption/luminescence spectra (Fig. S8 and Table S3). Herein, the frontier molecular orbitals involved in the excitation and the singlet/triplet excited states were selected. For CN-T (Fig. 6a and Table S4), there are singlet excitations from $S_0 \rightarrow S_1$, S_2, S_3 and S_4. The electronic components of both $S_0 \rightarrow S_1$ and $S_0 \rightarrow T_3$ transitions are HOMO → LUMO. The melem unit contributes to the HOMO, while the benzophenone moiety (spin converter) significantly contributes to the LUMO. Similar results can also be observed for ME-T (Fig. 6b and Table S5). These electronic components should benefit the ISC process.

Compared with melamine (Table S6), melem has a larger π conjugation resulting in relatively lower singlet and triplet energy levels (Table S7), especially for the singlet energy level. It would further benefit the decrease of the S_n energy level from CN-T. For example, the S_1 level of CN-T is 393 nm, which is lower than that of ME-T (S_1 = 370 nm). For the Tn energy level, there is also an impact, but with less extent, on CN-T (e.g. T_3 = 405 nm) and ME-T (e.g. T_3 = 393 nm). The ΔE_{ST} was calculated according to the excitation energy level of singlet and triplet excited states. It is shown from the calculation that the ΔE_{ST} of CN-T is only 0.09 eV, which is much smaller than ME-T (ΔE_{ST} = 0.2 eV). The smaller ΔE_{ST} benefits the energy of ISC from the singlet state to triplet state. It can then be used to sensitize the $^3O_2$ into $^1O_2$ through triplet–triplet energy transfer. Therefore, the results of theoretical calculations also suggest that the introduction of a proper ligand (melem) and spin converter (BTDA) would favor the ISC process and hence efficient $^1O_2$ generation.

4. Conclusions

In summary, some organic molecules exhibit a high yield of ISC, which can improve the efficiency of the ISC process in many conjugated polymers and enhance $^1O_2$ generation. In our study, we successfully prepared the heavy atom-free spin converter doped carbon nitride via the facile copolymerization of benzophenone and carbon nitride precursor. Time-resolved luminescence spectra demonstrated that the introduction of the benzophenone structure in BTDA can actually achieve energy level matching between the singlet state and triplet state, resulting in the reduction of ΔE_{ST} and hence generate $^1O_2$ effectively. In addition, DFT calculations also confirmed that the proper ligand (melem) would favor the ISC process and facilitate $^1O_2$ generation. In the photooxidation of 1,5-DHN, CN-T shows excellent photocatalytic selectivity, and the highest yield of Juglone can reach 71.8% after irradiation for 60 min, which was increased 1.3- times compared with cyclometalated Pt^{II} complexes (53.6%) in homogeneous photooxidation. This work may provide a feasible and effective strategy to selectively produce $^1O_2$ from carbon nitride and other conjugated polymers, which also helps widen the application of carbon nitride in the field of selective photooxidation.

Acknowledgments

This work was financially supported by NSFC (51672309, 21302224, 51172285 and 51372277), Shandong Provincial Natural Science Foundation (ZR2013BQ028 and ZR2013EMQ013), and the Fundamental Research Funds for Central Universities (18CX07009A, 15CX05010A, 15CX08005A and 15CX05013A). This work was performed, in part, at the Center for Nanoscale Materials, a U.S. Department of Energy Office of Science User Facility, and supported by the U.S. Department of Energy, Office of Science, under Contract No. DE-AC02-06CH11357.

Appendix A. Supplementary material

Supplementary data associated with this article can be found, in the online version, at https://doi.org/10.1016/j.jcat.2018.03.006.

References

[1] Y.Z. Chen, Z.U. Wang, H. Wang, J. Lu, S.H. Yu, H.L. Jiang, J. Am. Chem. Soc. 139 (2017) 2035–2044.
[2] T. Nakamura, A. Son, Y. Umehara, T. Ito, R. Kurihara, Y. Ikemura, K. Tanabe, Bioconjug. Chem. 27 (2016) 1058–1066.
[3] D. Kovalev, M. Fujii, Adv. Mater. 17 (2005) 2531–2544.
[4] X. Li, S. Kolemen, J. Yoon, E.U. Akkaya, Adv. Funct. Mater. 27 (2017) 1604053–1604063.
[5] W. Wu, X. Shao, J. Zhao, M. Wu, Adv. Sci. 4 (2017) 1700113–1700133.
[6] W. Wu, H. Guo, W. Wu, S. Ji, J. Zhao, Inorg. Chem. 50 (2011) 11446–11460.
[7] W. Wu, W. Wu, S. Ji, H. Guo, J. Zhao, Dalton Trans. 40 (2011) 5953–5963.
[8] S. Ji, H. Guo, W. Wu, W. Wu, J. Zhao, Angew. Chem. Int. Ed. 50 (2011) 8283–8286.
[9] W. Wu, Y. Geng, W. Fan, Z. Li, L. Zhan, X. Wu, J. Zheng, J. Zhao, M. Wu, RSC Adv. 4 (2014) 51349–51352.
[10] R. Wang, Y. Geng, L. Zhang, W. Wu, W. Fan, Z. Li, L. Wang, L. Zhan, X. Wu, M. Wu, Chin. J. Chem. 33 (2015) 1251–1258.
[11] H. Wang, S. Jiang, S. Chen, D. Li, X. Zhang, W. Shao, X. Sun, J. Xie, Z. Zhao, Q. Zhang, Y. Tian, Y. Xie, Adv. Mater. 28 (2016) 6940–6945.
[12] W. Wu, J. Zhang, W. Fan, Z. Li, L. Wang, X. Li, Y. Wang, R. Wang, J. Zheng, M. Wu, H. Zeng, ACS Catal. 6 (2016) 3365–3371.
[13] W. Zhang, A. Bariotaki, I. Smonou, F. Hollmann, Green Chem. 19 (2017) 2096–2100.
[14] S. Guo, L. Xu, K. Xu, J. Zhao, B. Küçüköz, A. Karatay, H.G. Yaglioglu, M. Hayvali, A. Elmali, Chem. Sci. 6 (2015) 3724–3737.
[15] H. Ünlü, E. Okutan, Dyes Pigments 142 (2017) 340–349.
[16] S. Hecht, J.M.J. Fréchet, J. Am. Chem. Soc. 123 (2001) 6959–6960.
[17] J. Zhao, W. Wu, J. Sun, S. Guo, Chem. Soc. Rev. 42 (2013) 5323–5351.
[18] R.R. Islangulov, D.V. Kozlov, F.N. Castellano, Chem Commun. (2005) 3776–3778.
[19] S. Ji, J. Yang, Q. Yang, S. Liu, M. Chen, J. Zhao, J. Org. Chem. 74 (2009) 4855–4865.
[20] S. Xu, Y. Yuan, X. Cai, C.J. Zhang, F. Hu, J. Liang, G. Zhang, D. Zhang, B. Liu, Chem. Sci. 6 (2015) 5824–5830.
[21] D.M.E. Freeman, A.J. Musser, J.M. Frost, H.L. Stern, A.K. Forster, K.J. Fallon, A.G. Rapidis, F. Cacialli, I. McCulloch, T.M. Clarke, R.H. Friend, H. Bronstein, J. Am. Chem. Soc. 139 (2017) 11073–11080.
[22] M. Etinski, C.M. Marian, Phys. Chem. Chem. Phys. 19 (2017) 13828–13837.

[23] S.J. Makowski, P. Kostler, W. Schnick, Chem. Eur. J. 18 (2012) 3248–3257.
[24] Y. Zheng, L. Lin, X. Ye, F. Guo, X. Wang, Angew. Chem. Int. Ed. 53 (2014) (1930) 11926–11931.
[25] X. Wang, K. Maeda, X. Chen, K. Takanabe, K. Domen, Y. Hou, X. Fu, M. Antonietti, J. Am. Chem. Soc. 131 (2009) 1680–1681.
[26] J. Zhang, Y. Chen, X. Wang, Energy Environ. Sci. 8 (2015) 3092–3108.
[27] J. Ran, T.Y. Ma, G. Gao, X.-W. Du, S.Z. Qiao, Energy Environ. Sci. 8 (2015) 3708–3717.
[28] J. Zhang, X. An, N. Lin, W. Wu, L. Wang, Z. Li, R. Wang, Y. Wang, J. Liu, M. Wu, Carbon 100 (2016) 450–455.
[29] X. Wang, W. Fang, W. Liu, Y. Jia, D. Jing, Y. Wang, L. Yang, X. Gong, Y. Yao, H. Yang, X. Yao, J. Mater. Chem. A 5 (2017) 19227–19236.
[30] S. Agrawal, A. Narula, Polym. Bull. 70 (2013) 3241–3260.
[31] J. Ge, M. Lan, B. Zhou, W. Liu, L. Guo, H. Wang, Q. Jia, G. Niu, X. Huang, H. Zhou, X. Meng, P. Wang, C.S. Lee, W. Zhang, X. Han, Nat. Commun. 5 (2014) 4596–4603.
[32] H. Wang, X. Yang, W. Shao, S. Chen, J. Xie, X. Zhang, J. Wang, Y. Xie, J. Am. Chem. Soc. 137 (2015) 11376–11382.
[33] S. Wang, L. Shang, L. Li, Y. Yu, C. Chi, K. Wang, J. Zhang, R. Shi, H. Shen, G.I. Waterhouse, S. Liu, J. Tian, T. Zhang, H. Liu, Adv. Mater. 28 (2016) 8379–8387.
[34] W. Wu, L. Zhan, W. Fan, J. Song, X. Li, Z. Li, R. Wang, J. Zhang, J. Zheng, M. Wu, H. Zeng, Angew. Chem. Int. Ed. 54 (2015) 6540–6544.
[35] K. Ishibashi, A. Fujishima, T. Watanabe, K. Hashimoto, Electrochem. Commun. 2 (2000) 207–210.
[36] W. Wu, P. Yang, L. Ma, J. Lalevée, J. Zhao, Eur. J. Inorg. Chem. 2013 (2013) 228–231.
[37] G. Zhang, G.M. Palmer, M.W. Dewhirst, C.L. Fraser, Nat. Mater. 8 (2009) 747–751.
[38] E. Yu-Tzu Li, T.Y. Jiang, Y. Chi, P.T. Chou, Phys. Chem. Chem. Phys. 16 (2014) 26184–26192.
[39] W. Wu, X. Wu, J. Zhao, M. Wu, J. Mater. Chem. C 3 (2015) 2291–2301.